

Chapter 2

Aspects and Investigation of Photochemical Dynamics

This chapter starts by reviewing concepts that form a versatile means of describing nuclear motion and electronic structure changes during a photochemical reaction. This is followed by an introduction of a framework capable of describing how such ultrafast photodynamics can be probed experimentally. Rather than extensively reproducing formulas [1], the intention is to highlight and qualitatively discuss selected issues relevant to this project. As such, this chapter serves as a reference for the rest of the thesis.

2.1 Photochemical Reaction Mechanisms

As of yet, the amount of literature on mechanistic photochemistry in general and ultrafast dynamics in particular is enormous. Some well-written examples can be found in Refs. [2–8] and this section is intended to be an extract of those works. Unless otherwise stated only singlet electronic states are dealt with in the following.

2.1.1 *The Photochemical Funnel*

In 1935 Eyring [9], Evans and Polanyi [10] clarified the nature of the transition state and defined the reaction path of a ground state (thermal) chemical reaction. Today the basic mechanistic concepts are familiar to any chemist: being a first-order saddle point on the ground state PES, the transition state is the maximum along a single well-defined (although potentially complex) reaction coordinate connecting the reactants and products as local minima on the PES.

In photochemical reactions the picture is not as clear: although excited-state product formation has been observed [11, 12], most often the chemical transformation occurs in structures for which an excited-state PES is energetically close to or

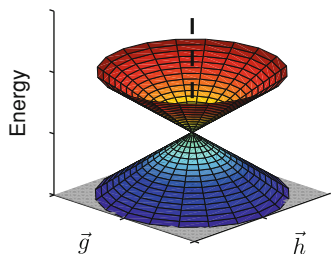


Fig. 2.1 Sketch displaying two PESs against the gradient difference (\vec{g}) and derivative coupling (\vec{h}) nuclear displacement coordinates spanning the *branching space* (gray) that defines a conical intersection. These coordinates lift the degeneracy of the surfaces linearly, while it is maintained in the *seam space* consisting of the nuclear displacement coordinates orthogonal to the branching space (represented by the *dashed line* through the cone)

degenerate with the ground state PES [13, 14]. The most common type of intersection of PESs is the conical intersection (CI), which is often called a photochemical ‘funnel’ [8, 15], through which reactions can happen. As such, CIs play the same decisive role for the mechanism in photochemical reactions as transition states do in ground state reactions; the first direct experimental support of this statement was recently obtained by Polli et al. [16] The intersection is named conical because the intersecting PESs form a double cone when displayed against the two *branching space* coordinates, called the *gradient difference* (\vec{g}) and the *derivative coupling* (\vec{h}), as shown in Fig. 2.1. Mathematically, the coordinates are defined as [13]

$$\vec{g} = \frac{\partial(E_2 - E_1)}{\partial \mathbf{R}} \quad \vec{h} = \langle \phi_1 | \frac{\partial \hat{H}}{\partial \mathbf{R}} | \phi_2 \rangle \quad (2.1)$$

in which \mathbf{R} represents the nuclear coordinates, E_1 and E_2 are the PESs of the $|\phi_1\rangle$ and $|\phi_2\rangle$ states, respectively, and \hat{H} is the Hamilton operator. This illustrates a fundamental difference between a CI and a ground state transition state in terms of the ‘reaction coordinate space’. At a CI this space is spanned by the two branching space coordinates rather than the single reaction coordinate defining the ground state reaction. As a consequence, while passage through a transition state in the ground state leads to a single product, passage through a CI can lead to two or more products depending on the number of accessible valleys on the ground state PES [13]. The reaction paths taken are determined by the topography of the PESs at the CI [14, 17–19] as well as the velocities of the nuclei along \vec{g} and \vec{h} , as discussed below.

Note that while the branching space coordinates lift the degeneracy of the PESs linearly, it is maintained in the rest of the nuclear displacement coordinates (at least to first order). Thus, there will be another CI at a structure slightly displaced along any of the latter coordinates, called the *seam space*. In a nonlinear molecule containing N atoms the dimension of the seam will be $3N - 6 - 2 = 3N - 8$, which means that in a three-atom nonlinear molecule the seam is a line. This clearly shows that,

already for small molecules, there is another increase in complexity as compared to the ground state reaction with one well-defined transition state: the photochemical reaction can occur through an infinite number of ‘transition states’ along this line. This complexity is reduced when one considers the lowest-energy structure within the seam, the minimum-energy CI (MECI): analogously to the minimum-energy path in the ground state, one might think that in a photochemical reaction the molecule follows a minimum-energy path in the excited state between the Franck–Condon structure and the MECI. While this is an appealing and intuitively simple picture, it is not always capturing the most important pathway leading to the photochemical reactivity. Therefore it is in some cases necessary to embrace the complexity and take into account a whole range of CIs [20].

2.1.2 Non-Adiabatic Dynamics

The reason for the importance of CIs and for their naming as *funnels* is that internal conversion (IC), nonradiative transition from one electronic state to another of the same spin multiplicity, is extremely efficient at a CI. This means that the process is very competitive towards other (non-reactive) decay channels such as electronic transitions involving a change of spin multiplicity or emission of a photon.

Another way of stating that the rate of nonradiative transition is high is that the coupling between the electronic states is large. Since it is important to appreciate why this is so, the following serves to remind the reader of the origin of the coupling by discussing the scenario sketched in Fig. 2.2. When PESs are well separated, the coupling between the movement of the nuclei and the electrons can be neglected and their interaction assumed adiabatic. In other words, the electrons are assumed to move infinitely fast, instantaneously adapting to the electric field from the nuclei. But when the transition frequency corresponding to the energy difference between the PESs becomes comparable to the frequency of the changing electric field from the moving nuclei, the electrons can no longer keep up. Their interaction with the nuclei is now non-adiabatic: nuclear movement can induce electronic transitions, converting kinetic into potential energy or vice versa. This nonradiative transition occurs on the timescale of the nuclear motion and is therefore ultrafast. Because it is a consequence of a non-adiabatic interaction between the nuclei and the electrons, such a transition is classified as non-adiabatic and the effect mediating it is termed non-adiabatic coupling.

In a quantum mechanical description, it is the nuclear kinetic energy operator that is responsible for the coupling between two adiabatic states. Therefore, the non-adiabatic coupling operator [21] that determines the transition probability between the states includes the derivatives with respect to nuclear position of both the electronic and nuclear part of the wave function. The former derivative is a measure of the extent of electronic character change when the nuclei are moved, from which it can be appreciated that in regions of high non-adiabatic coupling, the electronic character depends heavily on nuclear displacement. Therefore the coupling

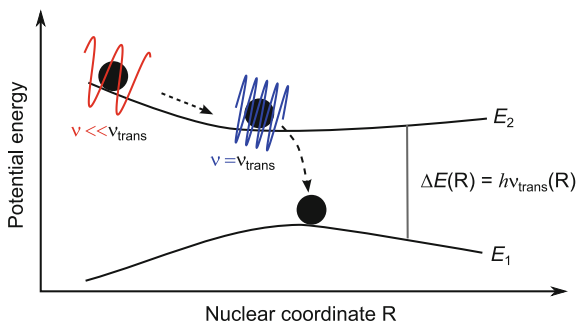
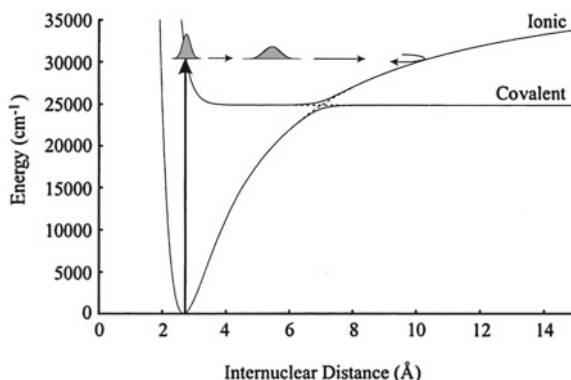


Fig. 2.2 Sketch illustrating the phenomenon of non-adiabatic dynamics. When the PESs E_1 and E_2 are far apart, the interaction between the electrons and nuclei is adiabatic. But when the nuclei have gained speed and encounter a region where the PESs are close, the rate of change of the electric field from the nuclei is comparable to the transition frequency ν_{trans} between the PESs. This means that the interaction between nuclei and electrons is non-adiabatic: nuclear motion can induce a nonradiative electronic transition

diverges to infinity at a CI but more importantly remains large in the vicinity of the intersection. This means that IC is efficient in all molecular structures within that vicinity. Whether a structure can be considered in ‘the vicinity’ depends not only on the static PESs but also on the velocity of the nuclei, when the molecule passes by the CI. Thus, the CI is a convenient concept of a reaction funnel in the description of photochemistry, but in reality the funnel also includes structures in the surroundings of the CI. In short, the (minimum-energy) CI should not be considered the holy grale of photochemistry: if at any time the speed of the nuclei causes their electric field to change at a rate comparable to the transition frequency between the PESs, non-adiabatic dynamics will occur (and have just the same potential for leading to photochemical reactions as CIs do). In fact, in diatomic molecules the PESs of two states of the same symmetry cannot intersect [22], but non-adiabatic dynamics can still happen in regions where they come close, called avoided crossings. Even in polyatomic molecules avoided crossings can occur, but they are not as frequent as CIs [23]. This can be appreciated by considering the cone shown in Fig. 2.1 and making a cut that does not go through the center of the cone. In this cut the PESs will exhibit what looks like an avoided crossing, but does not classify as a *true* avoided crossing, since in the latter case there is not a CI nearby.

The photodissociation of NaI investigated by Zewail and coworkers is a classical example of non-adiabatic dynamics in general and electronic transition at an avoided crossing in particular [24–26]. The PESs of the ground and first excited states are displayed in Fig. 2.3: as can be seen, there is an avoided crossing between the PESs near an internuclear distance of 7 Å. In this region the electronic character of the states—ionic or covalent bonding—changes dramatically as a function of internuclear distance, and the experiment was able to probe the non-adiabatic dynamics of the photodissociation following electronic transition between the first excited state and the ground state [24, 25].

Fig. 2.3 The PESs of the ground and first excited states of NaI. Near the avoided crossing around 7 Å the electronic character of the states—ionic or covalent bonding—is heavily dependent on the internuclear distance. When this region of the PESs is encountered non-adiabatic coupling induces an electronic transition followed by photodissociation. Figure 1 in Ref. [26]



2.1.3 Intersystem Crossing

This chapter is focused on excited singlet states, since these are optically active and IC between such states is often much faster than intersystem crossing (ISC); the electronic transition between states of different spin multiplicity. The reason is that whereas IC is induced by the non-adiabatic coupling, it is (generally) the interaction between the spin and the orbital angular momentum of the electrons, the spin-orbit coupling, that induce ISC. In many organic molecules not containing heavy atoms this coupling is weak, corresponding to a low rate of ISC compared to IC. But through a series of studies El-Sayed [27–29] discovered that in cases where the transition occurs from a (n, π^*) to a (π, π^*) state or vice versa, the rate is significantly increased. These transitions are often observed in carbonyl compounds, and this thesis will present experiments on such a compound (Chap. 8) in which ISC even outcompetes IC to the ground state. Readers interested in a thorough review of the physics of ISC are referred to the discussion by Turro et al. (pp 146–156, Chapter 3 in Ref. [8]).

2.1.4 Ultrafast Reactivity

The fact that ultrafast reactivity is closely linked to non-adiabatic dynamics can be appreciated by considering that not only the change of electronic character, but also the velocity of the nuclei determines the magnitude of the non-adiabatic coupling and thereby the probability of electronic transition. Although it is not the complete picture, some intuition can be gained from the Landau–Zener model (see Ref. [30] for Zener’s original paper) of radiationless transitions; Desouter-Lecomte and Lorquet derived the following one-dimensional expression for the transition probability between two adiabatic electronic states I and J [31]

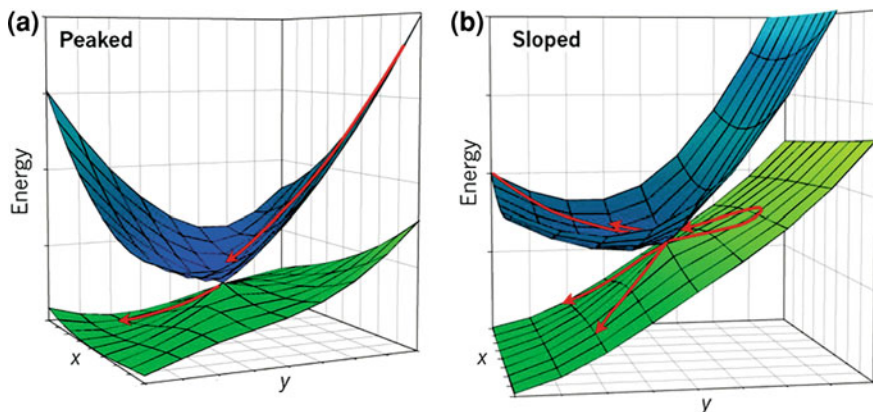


Fig. 2.4 Illustration of the course of non-adiabatic dynamics at two different types of CIs, classified according to their topography in the branching space (x, y) . **a** the nuclear trajectories are directed toward the CI, resulting in a very efficient electronic transition. **b** the net rate of electronic transition is decreased due to an increased probability of nuclear trajectories returning from the lower to the upper PES, as illustrated by the upper *red arrow*. Figure 1 in Ref. [19]

$$P_{IJ} = \exp[-(\pi/4)\xi] \quad \xi = \frac{\Delta E(\vec{q})}{\hbar|\dot{\vec{q}}||\vec{\lambda}_{IJ}(\vec{q})|} \quad (2.2)$$

where ξ is called the Massey parameter. ΔE is the energy difference between the PESs of the two states, the overdot indicates the time derivative and \vec{q} is a nuclear displacement vector parallel to $\vec{\lambda}_{IJ}$, the non-adiabatic coupling between the states

$$\vec{\lambda}_{IJ} = \langle \phi_I | \frac{\partial}{\partial \vec{q}} | \phi_J \rangle \quad (2.3)$$

which is parallel to the derivative coupling \vec{h} [13]. In the framework of Eq. (2.2) the transition probability increases with decreasing energy difference and is one at a CI. Importantly the transition probability also depends on the product between the speed along \vec{q} and the magnitude of the non-adiabatic coupling. Therefore the largest transition probability is obtained if the nuclei move parallel to \vec{h} . Considering the case of a molecule approaching a CI this means that not only should the speed of the nuclei be large, the velocity should also have a component along \vec{h} for a transition to occur. The larger the magnitude of this component, the greater the probability of the transition. The role of the CI as a funnel in a photochemical reaction can now be further elaborated. The CI acts as a filter in the position-momentum phase space: the magnitude and direction of $\vec{\lambda}_{IJ}$ determines the velocity distribution of events leading to electronic transition and thereby photochemical reaction. But the magnitude of $\vec{\lambda}_{IJ}$ generally increases with decreasing energy difference, why movement along the gradient difference \vec{g} will also influence the transition probability (although this is not contained in the one-dimensional Landau–Zener model). If, as shown in Fig. 2.4a,

the topography of the PESs at the CI directs the molecule to that favorable region of the phase space, the transition probability is very high or in other words the electronic transition is ultrafast: within a single vibrational period [32]. Such a CI topography is classified as *peaked* [19]. On the other hand, if the topography is such that the center axis of the CI is tilted, Fig. 2.4b, the CI is classified as *sloped* [19]. The net rate of transition is expected to be decreased at a sloped CI, because of an increased probability of nuclear trajectories crossing back from the lower to the upper PES. Whereas the transition probability at a CI increases with the speed along the branching space coordinates, experimental results obtained by Lee et al. [33] lead them to suggest that increased speed along the seam space coordinates can in fact decrease the transition probability at a sloped CI. Hence, the rate of IC at a sloped CI is governed by the relative speeds of the nuclei along the branching and seam space coordinates, respectively.

Summing up the above in a less rigorous way, very efficient electronic transitions are mediated by passage through (the vicinity of) a CI when specific nuclear degrees of freedom are activated. Because of the high efficiency ultrafast reactivity cannot be described by a kinetics model that is inherently statistical (although often this is actually what is done when experimental data is fitted!). This places ultrafast photochemical reactivity in sharp contrast to a thermal reaction in the ground state in which the probability of passing through the transition state is low, making ground state reactions well described by kinetic models such as Eyring, Evans and Polanyi's transition state theory mentioned above. The non-statistical nature of ultrafast photochemical processes is what makes them so exciting, and in the quest to understand how the absorbed photon energy is distributed among electrons and nuclei, much can be learned about fundamental chemical problems.

2.2 Probing Ultrafast Dynamics: The Pump–Probe Principle

When designing an experimental setup for investigating ultrafast dynamics of chemical transformations the experimentalist has to fulfill two requisites: an ultrashort probe with a duration of fs and a way to clock it to a trigger with the same time-resolution. Presently, there exist several schemes that comply to these requirements. Common to all of them is the pump–probe principle in which an ultrashort optical pulse, the pump, initiates a chemical change in the sample. A well-defined time-delay after that event an ultrashort probe measures a given property of the sample. By recording this property at a series of delays, time-dependent information about the initiated dynamics is obtained. Depending on the question that the experiment is designed to answer, different probes are used. Using ultrashort X-ray and electron pulses direct structural information can be obtained from diffraction patterns [34, 35], whereas optical probe pulses provide spectroscopic information. Here we will focus on the use of the latter in the field of ultrafast time-resolved spectroscopy. More specifically, unless otherwise stated, experiments involving absorption of one photon of the pump and one photon of the probe pulse are considered.

2.2.1 Coherence

The fundamental difference between time-resolved and steady state spectroscopy stems from the characteristics of the lasers used. From the Fourier relationship between the time and frequency domain it becomes clear that the infinite duration of the continuous wave (CW) lasers used in steady state spectroscopy, corresponds to a monochromatic wavelength spectrum. In time-resolved spectroscopy the situation is different: a finite (ultrashort) pulse duration in the time domain corresponds to a finite bandwidth in the frequency domain. It is important to realize that a finite spectral bandwidth in itself does not lead to a finite duration in the time domain: light from the sun is not pulsed despite the large bandwidth of frequencies emitted. The reason is that the frequencies from the sun are emitted at random instances in time. Another way of stating this is that the phases of the spectral components are not synchronized. The role of phase relationship can be illustrated with a simple example.

Considering the transversal modes of a laser cavity, there is (for most laser media) a set of modes with different frequencies that experience a gain that is greater than the cavity losses. Thus, these modes can exist simultaneously in the cavity and it is therefore instructive to consider the electric field generated by a superposition of these modes. For simplicity we assume the modes to be linearly polarized in the same direction so that a scalar expression of the modes is appropriate

$$e_i(t) = E_i \cos[\omega_i t + \varphi_i(t)] \quad (2.4)$$

where E_i is the field amplitude, ω_i is the frequency and $\varphi_i(t)$ is a time-dependent phase-factor of the i th mode. Figure 2.5 illustrates how the relationship between the latter factors will determine the time-dependence of the intensity, $I(t) = (\sum_{i=1}^N e_i(t))^2$, of the electric field generated by a superposition of N of these modes in the cavity. Figure 2.5a shows the result obtained from one mode and Fig. 2.5b that of two modes in phase, $\varphi_1(t) = \varphi_2(t)$. Figure 2.5c shows the result obtained from six modes with random phases, whereas Fig. 2.5d shows that of the same six modes with fixed phase relationships, $\varphi_i(t) = \varphi_j(t)$ for all i and j .

The main lesson to be learned from Fig. 2.5 is that when the phases of the modes are synchronized they interfere to generate well-defined time-dependent maxima of the intensity, whereas if there is no relationship between the phases the intensity varies randomly. When synchronized in phase the modes are called *coherent*. Thus, the sun is an incoherent light source, since there is no fixed relation between the phases of the emitted frequencies. Furthermore, comparison of Fig. 2.5b and d illustrates that coherence is crucial for making ultrashort laser pulses: the more cavity modes that can be synchronized in phase the shorter the pulse. The reader is referred to Ref. [36] for a thorough description of ultrashort laser pulses and how phase synchronization is achieved in practice.

Finally, note that while each mode is a standing wave, their coherent superposition is a *wave packet* that travels back and forth in the cavity. This can be shown completely

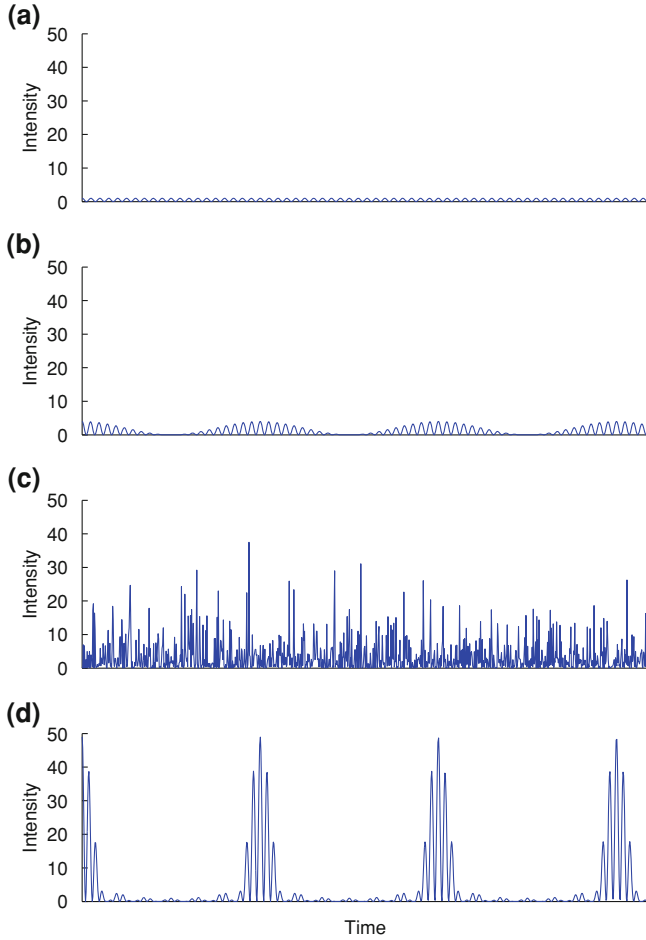


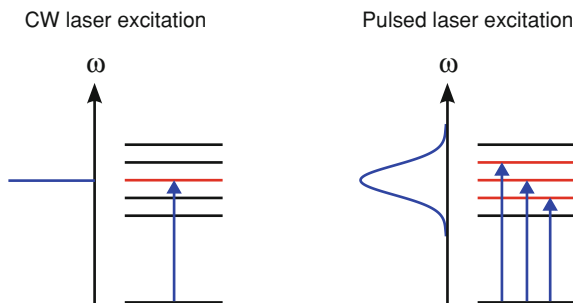
Fig. 2.5 Illustration of how the phase relations between a set of modes, $e_i(t) = E_i \cos[\omega_i t + \varphi_i(t)]$, influence the time-dependent intensity, $I(t) = (\sum_{i=1}^N e_i(t))^2$, of the field resulting from their superposition. **a** $N = 1$ mode. **b** $N = 2$ modes in phase, $\varphi_1(t) = \varphi_2(t)$. **c** $N = 6$ modes with random phases. **d** $N = 6$ modes synchronized in phase, $\varphi_i(t) = \varphi_j(t)$ for all i, j

analogously to what was done above in the time domain, by including the spatial dimension in the expression of the transversal modes.

2.2.2 Pump: Creation of a Wave Packet

Having established the concept of coherence, this section serves to explain why coherence plays a crucial role in the excitation step of a pump-probe experiment.

Fig. 2.6 Illustration of how absorption of a photon from a CW laser excites a single eigenstate (*left*), whereas an ultrashort laser pulse excites a coherent superposition of eigenstates (*right*)



First, a comparison between the well-known steady state and the ultrafast time-resolved spectroscopy is instructive. Thus, consider Fig. 2.6 that sketches a one-photon excitation of a ground state molecule by a CW and an ultrafast pulsed laser, respectively. Focusing on the CW excitation of a steady state experiment first, the single frequency component of the laser excites a single eigenstate of the molecule. The norm and any expectation value of an eigenstate is constant in time, which is why eigenstates are often called stationary states. Turning to the pump-probe experiment, an ultrashort laser pulse excites a set of eigenstates contained within the spectral bandwidth of the pulse. Because the phases of the spectral components within this bandwidth are synchronized, the excitation leads to a coherent superposition of stationary states constituting a wave packet $|\Psi(t)\rangle$. This terminology is not coincidental and in the following it will be clear that a wave packet of eigenstates is conceptually quite similar to the wave packet of laser modes discussed above. In view of clarity, assume the wave packet to be comprised of two stationary states $|a\rangle$ and $|b\rangle$ excited simultaneously and in equal amplitude

$$|\Psi(t)\rangle = \frac{1}{\sqrt{2}} \left(e^{-iE_a t/\hbar} |a\rangle + e^{-iE_b t/\hbar} |b\rangle \right) \quad (2.5)$$

where E_a and E_b are the energies of the eigenstates. Note that as opposed to the two terms it is comprised of, the wave packet itself is *not* an eigenstate of the time-dependent Schrödinger equation. By considering the expectation value of the wave packet for a given operator \hat{X} , it becomes clear that it is time-dependent [1]

$$\langle \Psi(t) | \hat{X} | \Psi(t) \rangle = \frac{1}{2} \left(\langle a | \hat{X} | a \rangle + \langle b | \hat{X} | b \rangle \right) + \cos[(E_b - E_a)t/\hbar] \langle a | \hat{X} | b \rangle \quad (2.6)$$

This expression illustrates that the coherence of the laser pulse is the key property for the success of the time-resolved experiment: because the stationary states are excited in phase, interference between the states leads to a time-dependent expectation value of the wave packet. In other words, the laser pulse has initiated dynamics in the molecule. In this simplified case of only two stationary states the dynamics is simply an oscillation about the average of the expectation values of each state. But in

more realistic examples in which several states are excited, and their amplitudes and phases are determined by both the transition dipole moment and the spectral components of the laser pulse, wave packets can exhibit significantly more complicated behavior.

In polyatomic molecules, the exact molecular eigenstates contained in the wave packet cannot be computed and even if they could, their coherent superposition would be incomprehensible. Thus, it is often useful to adapt a simpler and more intuitive basis in which to expand the exact eigenstates. As photochemical reactions is the subject of interest here, the adiabatic representation of electronic states mentioned earlier, is an obvious choice. In a typical experiment the wave packet will, at its birth, resemble a single excited electronic state, when expanded in that basis. As time goes by and the phase factors of the exact eigenstates evolve, the wave packet may then, when expanded in the adiabatic basis, turn out to have acquired character of a different electronic state. In the framework of adiabatic states this is a consequence of a non-adiabatic coupling between the electronic states, but it is stressed that the coupling is really a consequence of the choice of expansion basis. A different basis will provide a different view of what is of course the same dynamics. In any case, the expansion in simpler bases provides a more intuitive illustration of how the pump pulse can be used to trigger non-adiabatic dynamics such as a photochemical reaction with fs time-resolution.

2.2.3 Probe: Projection onto a Final State

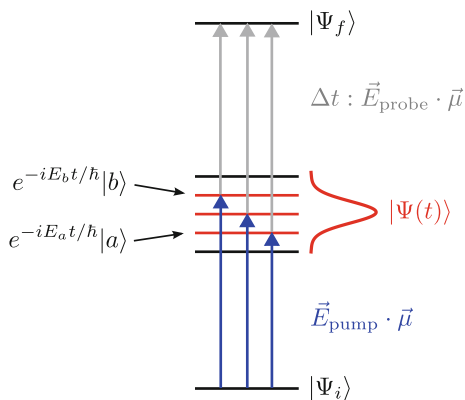
After its creation by the pump pulse, the wave packet $|\Psi(t)\rangle$ evolves freely for a time Δt after which a second laser pulse probes it by projection on a final state $|\Psi_f\rangle$ in a one-photon excitation, as sketched in Fig. 2.7. The differential signal resulting from excitation to that particular state can be expressed as [37]

$$S_f(\Delta t) = |\langle \Psi_f | \vec{E}_{\text{probe}}(\omega) \cdot \vec{\mu} | \Psi(\Delta t) \rangle|^2 \quad (2.7)$$

in which $\vec{E}_{\text{probe}}(\omega)$ is the Fourier transform of the electric field of the probe pulse at the transition frequency ω (this is elaborated on in Sect. 4.2.3) and $\vec{\mu}$ is the transition dipole moment operator. Stolow and Underwood have rewritten Eq. (2.7) to a form that more clearly shows the signal to be comprised of interferences between energetically degenerate two-photon transitions to the final state [37]. For brevity the equation will not be written here, as the conclusion to draw is analogous to that drawn from Eq. (2.6); the experimental signal is modulated at frequencies corresponding to the energy differences between the stationary states within the wave packet.

In the probing step, the phase and amplitude of each of the stationary states are altered by the spectral components of the probe laser and the transition dipole moment to the final state. While the former contribution can be controlled, the latter depends on molecular structure and of course the final state itself. At a given time, there can

Fig. 2.7 Sketch illustrating the creation, evolution and probing of a wave packet. The experimental signal [see Eq. (2.7)] will be modulated at frequencies corresponding to the energy differences between the stationary states comprising the wave packet, resulting from interferences between energetically degenerate two-photon transitions such as those indicated in the figure



be a large overlap to one final state and a small overlap to another, while at a later time the situation is reversed. This illustrates that the final state acts as a template that the wave packet is projected onto by excitation with the probe pulse. As in every projection, information is lost in the process. But, when choosing different final states one has the possibility of making different projections and thereby hope to recover the (most important part of the) wave packet dynamics.

It is not always experimentally feasible to select a single final state, though, and the collected signal is integrated over a set of energetically allowed final states

$$S(\Delta t) = \sum_f S_f(\Delta t) \quad (2.8)$$

as is the case when measuring total fluorescence, total ion yield, etc. The integration done in such experiments may wash out the information about the wave packet dynamics available from each of the differential signals within the sum or even lead to false conclusions about the dynamics. Stolow and Underwood discuss an example of the latter case, comparing the integral detection of a total ion yield measurement with the differential detection of photoelectron spectroscopy [37].

2.2.4 Experimental Techniques

Even within the limited class of ultrafast experiments involving one optical pump and one optical probe pulse, several experimental schemes exist, e.g. time-resolved transient absorption spectroscopy [38], fluorescence spectroscopy [39], mass spectrometry (TRMS) [37, 39] and photoelectron spectroscopy (TRPES) [37, 39–49], to name a few. Every technique has its practical benefits and drawbacks, but most importantly from a conceptual point of view the final states are different. Thus, this property should (ideally) be the basis for the choice of a technique

for answering a specific scientific question, since it determines the experimental sensitivity towards different dynamics. In this project we have chosen TRMS and TRPES, since especially the latter offers appealing properties and is applicable in a large range of problems. These techniques belonging to time-resolved photoionization spectroscopy have some intriguing fundamental benefits as compared to the other techniques mentioned above, which will be discussed in Chap. 3.

2.3 What is Probed?

When conducting time-resolved experiments a major part of the time is spent on interpreting the results. In that process it is important to realize which factors can influence the experimental signal to ultimately answer the question of what the experiment really probes. This section will mention two such factors

The final state acting as a filter through which the wave packet dynamics is probed.

Sample averaging due to e.g. different environments or structures of the molecules in the sample.

2.3.1 The Final State

When designing a time-resolved experiment, one has to choose a (set of) final state(s) to act as the probing template. This choice should be done wisely, since it determines what information can be extracted from the experiment: it is the filter through which the dynamics is observed. In simple terms, if the experiment aims at answering if the molecule emits yellow light during the course of a chemical reaction, it should be made sure that the filter is indeed transparent to yellow light. The optimal choice of template reflects maximal sensitivity towards the dynamics of interest for the particular experiment. But in many cases too little is known about the final states to achieve this goal and a (more or less) qualified guess on a suitable final state is made. In such situations the interpretation of the experimental signals involves modeling of which molecular parameters the template can be expected to be sensitive to, and which of them are involved in the dynamics studied. Eventually, a close connection to advanced theory is necessary to raise the models to a level above qualified guesses or even to prevent false conclusions. This subject will be touched upon in Part II.

2.3.2 Sample Averaging

So far the attention was drawn to the probing step in a single molecule. Although it is practically possible to do single-molecule experiments [50, 52], most ultrafast

spectroscopy experiments are conducted on samples containing several molecules. Thus, it is important to realize how sample averaging influences the experimental signal. In experiments on molecules in solution the Boltzmann population of vibrational states and the influence of solvent on the local environment of each molecule is an example of such averaging. When conducting time-resolved experiments on molecules in gas phase as in this project, the use of a molecular beam considerably reduces the averaging by cooling the isolated molecules vibrationally and rotationally. But even in gas phase experiments averaging can arise due to the presence of different conformers in the molecular beam. In the time-resolved experiments on [2+2]cycloaddition conducted in this project (Chap. 7), it was possible to extract the contribution of two different conformers from the experimental signal, because of very different time scales of their dynamics, but in general this is not possible. Thus, it is desirable to be able to conduct the experiments on single conformers [53] to get the cleanest possible picture of the molecular dynamics. Recently, spatial separation of conformers in a molecular beam was demonstrated by Filsinger et al. using a very simple technique of deflection in a static electric field [54], but so far it has not been used for time-resolved experiments on conformationally pure samples.

References

1. Brogaard, R.Y.: Teoretiske og eksperimentelle undersøgelser af ultrahurtig dynamik. M. Sc. thesis, University of Copenhagen, In Danish. <http://dl.dropbox.com/u/2637141/MscThesisRasmusBrogaard.pdf> (2008)
2. Gilbert, A., Baggott, J.: *Essentials of Molecular Photochemistry*. Blackwell Scientific Publications, Boston (1991)
3. Schinke, R.: *Photodissociation Dynamics*. Cambridge Monographs on Atomic, Molecular, and Chemical Physics 1. Cambridge University Press, Boston (1993)
4. Horspool, W.M., Song, P.-S. (eds.): *CRC Handbook of Organic Photochemistry and Photobiology*. CRC Press, Inc., Boca Raton (1995)
5. May, V., Kühn, O.: *Charge and Energy Transfer Dynamics in Molecular Systems*. Wiley-VCH, Berlin (2000)
6. Domcke, W., Yarkony, D.R., Köppel, H. (eds.): *Conical Intersections: Electronic Structure, Dynamics and Spectroscopy*. World Scientific Publishing Co. Pte. Ltd., Singapore (2004)
7. Tannor, D.J.: *Introduction to Quantum Mechanics—A Time-Dependent Perspective*. University Science Books, Sausalito (2007)
8. Turro, N.J., Ramamurthy, V.J.C.: *Modern Molecular Photochemistry of Organic Molecules*. University Science Books, Scaiano (2010)
9. Eyring, H.: *Chem. Rev.* **17**, 65–77 (1935)
10. Evans, M.G., Polanyi, M.: *Trans. Faraday Soc.* **31**, 875–894 (1935)
11. Turro, N.J., Lechtken, P., Lyons, A., Hautala, R.R., Carnahan, E., Katz, T.J.: *J. Am. Chem. Soc.* **95**, 2035–2037 (1973)
12. De Waele, V., Beutler, M., Schmidhammer, U., Riedle, E., Daub, J.: *Chem. Phys. Lett.* **390**, 328–334 (2004)
13. Bernardi, F., Olivucci, M., Robb, M.A.: *Chem. Soc. Rev.* **25**, 321–328 (1996)
14. Migani, A., Olivucci, M.: *Conical Intersections: Electronic Structure, Dynamics and Spectroscopy*. In: Domcke, W., Yarkony, D.R., Köppel, H. (eds.) *Conical Intersections and, Organic*

- Reaction Mechanisms, Chap 6, pp 272–315. World Scientific Publishing Co. Pte. Ltd., Singapore (2004)
15. Klessinger, M., Michl, J.: Excited States and Photochemistry of Organic Molecules. VCH Publishers Inc., New York (1995)
 16. Polli, D., Altoe, P., Weingart, O., Spillane, K.M., Manzoni, C., Brida, D., Tomasello, G., Orlandi, G., Kukura, P., Mathies, R.A., Garavelli, M., Cerullo, G.: *Nature* **467**, 440–443 (2010)
 17. Atchity, G.J., Xantheas, S.S., Ruedenberg, K.: *J. Chem. Phys.* **95**, 1862–1876 (1991)
 18. Yarkony, D.R.: *J. Chem. Phys.* **114**, 2601–2613 (2001)
 19. Martinez, T.J.: *Nature* **467**, 412–413 (2010)
 20. Migani, A., Robb, M.A., Olivucci, M.: *J. Am. Chem. Soc.* **125**, 2804–2808 (2003)
 21. Cederbaum, L.S.: Conical Intersections: Electronic Structure, Dynamics and Spectroscopy. In: Domcke, W., Yarkony, D.R., Köppel, H. (eds.) *Born-Oppenheimer Approximation and Beyond*, Chap 1, p 6. World Scientific Publishing Co. Pte. Ltd., Singapore (2004)
 22. von Neumann, J., Wigner, E.P.Z.: *Physik* **30**, 467–470 (1929)
 23. Truhlar, D.G., Mead, C.A.: *Phys. Rev. A* **68**, 032501 (2003)
 24. Rose, T.S., Rosker, M.J., Zewail, A.H.: *J. Chem. Phys.* **88**, 6672–6673 (1988)
 25. Mokhtari, A., Cong, P., Herek, J.L., Zewail, A.H.: *Nature* **348**, 225–227 (1990)
 26. Møller, K.B., Henriksen, N.E., Zewail, A.H.: *J. Chem. Phys.* **113**, 10477–10485 (2000)
 27. El-Sayed, M.A.: *J. Chem. Phys.* **36**, 573–574 (1962)
 28. El-Sayed, M.A.: *J. Chem. Phys.* **38**, 2834–2838 (1963)
 29. El-Sayed, M.A.: *J. Chem. Phys.* **41**, 2462–2467 (1964)
 30. Zener, C.: *Proc. R. Soc. London, Ser. A* **137**, 696–702 (1932)
 31. Desouter-Lecomte, M., Lorquet, J.C.: *J. Chem. Phys.* **71**, 4391–4403 (1979)
 32. Köppel, H., Cederbaum, L.S., Domcke, W., Shaik, S.S.: *Angew. Chem. Int. Ed. Engl.* **22**, 210–224 (1983)
 33. Lee, A.M.D., Coe, J.D., Ullrich, S., Ho, M.-L., Lee, S.-J., Cheng, B.-M., Zgierski, M.Z., Chen, I.-C., Martinez, T.J., Stolow, A.: *J. Phys. Chem. A* **111**, 11948–11960 (2007)
 34. Chergui, M., Zewail, A.H.: *Chem. Phys. Chem.* **10**, 28–43 (2009)
 35. Shorokhov, D., Zewail, A.H.: *J. Am. Chem. Soc.* **131**, 17998–18015 (2009)
 36. Rullière, C.: *Femtosecond Laser Pulses. Principles and Experiments*. Springer, Berlin (1998)
 37. Stolow, A., Underwood, J.G.: In: Rice, S.A. (ed.): *Advances in Chemical Physics*, vol. 139, pp. 497–584. Wiley, New York (2008)
 38. Nibbering, E.T., Fidler, H., Pines, E.: *Annu. Rev. Phys. Chem.* **56**, 337–367 (2004)
 39. Hertel, I.V., Radloff, W.: *Rep. Prog. Phys.* **69**, 1897–2003 (2006)
 40. Seel, M., Domcke, W.: *J. Chem. Phys.* **95**, 7806–7822 (1991)
 41. Kim, B., Schick, C.P., Weber, P.M.: *J. Chem. Phys.* **103**, 6903–6913 (1995)
 42. Neumark, D.M.: *Annu. Rev. Phys. Chem.* **52**, 255–277 (2001)
 43. Seideman, T.: *Annu. Rev. Phys. Chem.* **53**, 41–65 (2002)
 44. Reid, K.L.: *Annu. Rev. Phys. Chem.* **54**, 397–424 (2003)
 45. Stolow, A.: *Annu. Rev. Phys. Chem.* **54**, 89–119 (2003)
 46. Stolow, A., Bragg, A.E., Neumark, D.M.: *Chem. Rev.* **104**, 1719–1758 (2004)
 47. Wollenhaupt, M., Engel, V., Baumert, T.: *Annu. Rev. Phys. Chem.* **56**, 25–56 (2005)
 48. Suzuki, T.: *Annu. Rev. Phys. Chem.* **57**, 555–592 (2006)
 49. Reid, K.L.: *Int. Rev. Phys. Chem.* **27**, 607–628 (2008)
 50. van Dijk, E.M.H.P., Hernando, J., García-López, J.-J., Crego-Calama, M., Reinhoudt, D.N., Kuipers, L., García-Parajó, M.F., van Hulst, N.F.: *Phys. Rev. Lett.* **94**, 078302 (2005)
 51. Hernando, J., van Dijk, E.M.H.P., Hoogenboom, J.P., García-López, J.-J., Reinhoudt, D.N., Crego-Calama, M., García-Parajó, M.F., van Hulst, N.F.: *Phys. Rev. Lett.* **97**, 216403 (2006)
 52. Hildner, R., Brinks, D., Stefani, F.D., van Hulst, N.F.: *Phys. Chem. Chem. Phys.* **13**, 1888–1894 (2011)
 53. Stolow, A.: *Nature* **461**, 1063–1064 (2009)
 54. Filsinger, F., Küpper, J., Meijer, G., Hansen, J.L., Maurer, J., Nielsen, J.H., Holmegaard, L., Stapelfeldt, H.: *Angew. Chem., Int. Ed.* **48**, 6900–6902 (2009)

Molecular Conformation and Organic Photochemistry

Time-resolved Photoionization Studies

Brogaard, R.Y.

2012, XVI, 124 p., Hardcover

ISBN: 978-3-642-29380-1